

## ARTICLE

# A Semi-Mechanistic Population Pharmacokinetic Model of Nusinersen: An Antisense Oligonucleotide for the Treatment of Spinal Muscular Atrophy

Konstantinos Biliouris<sup>1</sup>, Puneet Gaitonde<sup>1</sup>, Wei Yin<sup>2</sup>, Daniel A. Norris<sup>3</sup>, Yanfeng Wang<sup>3</sup>, Scott Henry<sup>3</sup>, Robert Fey<sup>3</sup>, Ivan Nestorov<sup>2</sup>, Stephan Schmidt<sup>1</sup>, Mark Rogge<sup>2</sup>, Lawrence J. Lesko<sup>1</sup> and Mirjam N. Trame<sup>1,\*</sup>

A pharmacokinetic (PK) model was developed for nusinersen, an antisense oligonucleotide (ASO) that is the first approved treatment for spinal muscular atrophy (SMA). The model was built with data from 92 nonhuman primates (NHPs) following intrathecal doses (0.3–7 mg) and characterized the PK in cerebrospinal fluid (CSF), plasma, total spinal cord, brain, and pons. The estimated volumes were 13.6, 937, 4.5, 53.8, and 2.11 mL, respectively. Global sensitivity analysis demonstrated that the CSF-to-plasma drug distribution rate ( $0.09 \text{ hour}^{-1}$ ) is a major determinant of the maximum nusinersen concentration in central nervous system (CNS) tissues. Physiological age-based and body weight-based allometric scaling was implemented with exponent values of  $-0.08$  and  $1$  for the rate constants and the volume of distribution, respectively. Simulations of the scaled model were in agreement with clinical observations from 52 pediatric phase I PK profiles. The developed model can be used to guide the design of clinical trials with ASOs.

*CPT Pharmacometrics Syst. Pharmacol.* (2018) 7, 581–592; doi:10.1002/psp4.12323; published online on 16 Aug 2018.

## Study Highlights

### WHAT IS THE CURRENT KNOWLEDGE ON THE TOPIC?

☑ Nusinersen (Spinraza) is an antisense oligonucleotide that is the first and only approved treatment for spinal muscular atrophy, a rare neuromuscular disorder. It is administered intrathecal and its site of action is the CNS. Nusinersen PKs in nonclinical and clinical subjects has not been entirely characterized.

### WHAT QUESTION DID THIS STUDY ADDRESS?

☑ This research has developed a semimechanistic modeling approach to characterize nusinersen population PKs in NHPs that were subsequently scaled-up to pediatrics to predict nusinersen PKs in pediatric patients with SMA.

### WHAT DOES THIS STUDY ADD TO OUR KNOWLEDGE?

☑ The current research findings improve the understanding of nusinersen's PKs especially within the CNS of NHPs. Integration of allometric scaling principles further enables the developed NHP model to be used to predict nusinersen PKs in pediatric patients.

### HOW MIGHT THIS CHANGE DRUG DISCOVERY, DEVELOPMENT, AND/OR THERAPEUTICS?

☑ The presented population PK model can help to optimize the design of subsequent clinical trials with nusinersen and/or other antisense oligonucleotides under drug development.

Spinal muscular atrophy (SMA) is a rare autosomal, recessive motor-neuron disease caused by the lack of the functional form of survival of motor neuron (SMN) protein. This disease leads to degeneration of motor neurons in the spinal cord and lower brainstem, resulting in skeletal muscle atrophy.<sup>1–3</sup> SMA is the most common genetic cause of infant death and has an incidence of 1 in 11,000 live births.<sup>4–6</sup> There are three types of SMA that vary significantly among age at onset and severity. Type I constitutes as a severe form, type II an intermediate form, and type III as a mild form of SMA. Depending

on the type and severity of the disease, the life expectancy of the patients can range from only 2 years (type I) to normal (type III). Patients may suffer from respiratory insufficiency or may be incapable of sitting, standing, or walking. Respiratory failure, which eventually results in death, may also emerge in severe SMA cases.

Healthy people carry two *SMN* genes, namely *SMN1* and *SMN2*. The former is responsible for expressing the majority of SMN protein, thereby securing the functionality of SMN protein, which is essential to motor neurons. *SMN2* gene

<sup>1</sup>Center for Pharmacometrics and Systems Pharmacology, Department of Pharmaceutics, College of Pharmacy, University of Florida, Orlando, Florida, USA; <sup>2</sup>Biogen Idec, Cambridge, Massachusetts, USA; <sup>3</sup>Ionis Pharmaceuticals Inc., Carlsbad, California, USA. \*Correspondence: Mirjam N. Trame (mtrame@cop.ufl.edu)

expression oftentimes results either in reduced SMN protein levels, which are insufficient for proper motor neuron functioning, or in a truncated and dysfunctional SMN protein form due to an inherent splicing issue.<sup>7–9</sup> Proper expression of the *SMN1* gene is, therefore, crucial to prevent SMA development. However, scientific evidence indicates that a homozygous mutation in the *SMN1* gives rise to a dysfunctional form of SMN protein.

Promising treatments are currently being explored,<sup>4,10,11</sup> such as neuroprotectants,<sup>12</sup> stem cell therapy,<sup>13,14</sup> gene therapy,<sup>15</sup> and antisense therapy.<sup>16</sup> Antisense therapy capitalizes on macromolecules called antisense oligonucleotides (ASOs) that are complementary to the mRNA of SMN protein. The ASOs bind to mRNA and correct the splicing issue associated with the *SMN2* gene, thereby boosting the levels of functional SMN protein derived from the *SMN2* gene.<sup>17</sup> One such ASO that recently received US Food and Drug Administration (FDA) approval for the treatment of SMA is nusinersen (molecular weight of 7.5 kDa). Given that the prime site of action is the central nervous system (CNS), and that large ASOs do not cross the blood-brain-barrier when administered systemically, nusinersen is administered via intrathecal (i.t.) injection. Upon administration, it distributes within the CNS and peripheral tissues, such as skeletal muscle, liver, and kidneys, and is primarily eliminated likely by urinary excretion.<sup>18</sup> However, at the time of conduct of the present work, nusinersen's CNS disposition upon i.t. administration posed a significant drug development challenge and mechanistic modeling of nusinersen could provide benefit in further understanding the CNS disposition. Therefore, the objective of this work was (i) to develop a population pharmacokinetic (PopPK) model for nusinersen taking known ASO tissue distribution into consideration using non-human primate (NHP) data and (ii) to scale the developed NHP pharmacokinetic (PK) model using allometric principles to predict nusinersen concentrations in pediatric patients with SMA, which constitute the target patient population.

## METHODS

### Subjects and study design

Nusinersen PK studies and sample analyses were performed by Ionis Pharmaceuticals Inc (Carlsbad, CA). A noncompetitive hybridization nuclease-based enzyme-linked immunosorbent assay (ELISA) method or an electrochemiluminescence (ECL) method was used to quantitate intact nusinersen in cerebrospinal fluid (CSF), plasma, and evaluated tissues. The hybridization nuclease-based ELISA assay includes a complementary sequence DNA probe containing dual labels at each end using a modification of a previously described assay.<sup>19</sup> The hybridization nuclease-based ELISA method was demonstrated to be sensitive, linear, reproducible, precise, accurate, and selective for nusinersen in plasma, tissues, and CSF of monkey. The sensitivity of the ELISA assay for nusinersen was 1.5 ng/mL in plasma and CSF and 15 ng/mL in tissues. The hybridization-based ECL assay includes two complementary sequence probes: a capture probe biotinylated on the 5'-end, and a detection probe with a ruthenium label on the 3'-end. The assay was considered specific for the parent compound. The ECL method was more sensitive than

ELISA, and demonstrated to be linear, reproducible, precise, accurate, and selective for nusinersen in the plasma and CSF of humans. The sensitivity of the ECL assay for nusinersen was 0.05 ng/mL in CSF.

A total of 55 male and 37 female cynomolgus monkeys were used for the PK studies. Average male age was 2.8 years (SD = 1.6) with a mean body weight (BW) of 2.9 kg (SD = 1.3), whereas average female age was 2 years (SD = 1.6) with a mean BW of 1.8 kg (SD = 0.86). A single dose study (study #1) and two multiple dose studies (studies #3 and #5) were conducted, wherein a fixed dose of nusinersen was administered via the i.t. route. Study #1 was 71 days of duration and study #3 was 183 days of duration, whereas study #5 was a long-term study of 1 year of duration. Study #1 consisted for a dose range of 1–7 mg of nusinersen, study #3 comprised of 10 weekly doses (dose range 0.3–3 mg), whereas study #5 comprised of administration of 4 weekly doses of 1 mg of nusinersen. The PK sampling of CSF and plasma, along with staggered terminal sampling of the spinal cord and brain tissues were carried out. A comprehensive illustration of all dosing and sampling times is provided in **Figure 1**.

Upon tissue collection, the spinal cord was subdivided into the cervical, thoracic, and lumbar spinal cord regions, whereas the brain was separated into the cerebellum, brain cortex, frontal cortex, hippocampus, putamen, temporal cortex, motor cortex, thalamus, and pons. The tissues were homogenized prior to the determination of total drug concentration. The density of all tissues was assumed to be 1.0 g/mL. Nusinersen PK was also conducted in three cynomolgus monkeys following intravenous (i.v.) bolus administration as part of study #5. Subsequently, clinical PK studies were carried out, wherein single and multiple i.t. bolus of nusinersen was administered to 23 pediatric male patients with SMA with a mean age of 6 years (SD = 4.4) and a mean BW of 25 kg (SD = 21) as well as to 28 pediatric female patients with SMA with a mean age of 5.8 years (SD = 4) and a mean BW of 23 kg (SD = 16). In these patients, serial CSF and plasma nusinersen concentrations were measured using an ELISA assay.

### Nonhuman primate population pharmacokinetic analysis

PopPK model development was performed using NONMEM 7.3 (GloboMax/ICON, Ellicott City, MD). Plasma PK data following i.v. administration of nusinersen in three cynomolgus monkeys was used to evaluate one-compartment, two-compartment, and three-compartment plasma PK models. The objective function value (OFV), goodness of fit (GOF) plots, and visual predictive checks (VPCs) were used for model selection.

Upon the selection of the plasma PopPK model, PK data from various collected tissues of the i.t. dosing studies from 89 subjects were utilized to expand the plasma PK model and led to the development of the final NHP PopPK model. The model was built based on the following assumptions: (i) due to the sparseness of time-staggered PK measurements in the cerebellum, brain cortex, frontal cortex, hippocampus, putamen, temporal cortex, motor cortex, and thalamus regions of the brain, these tissues were combined to be

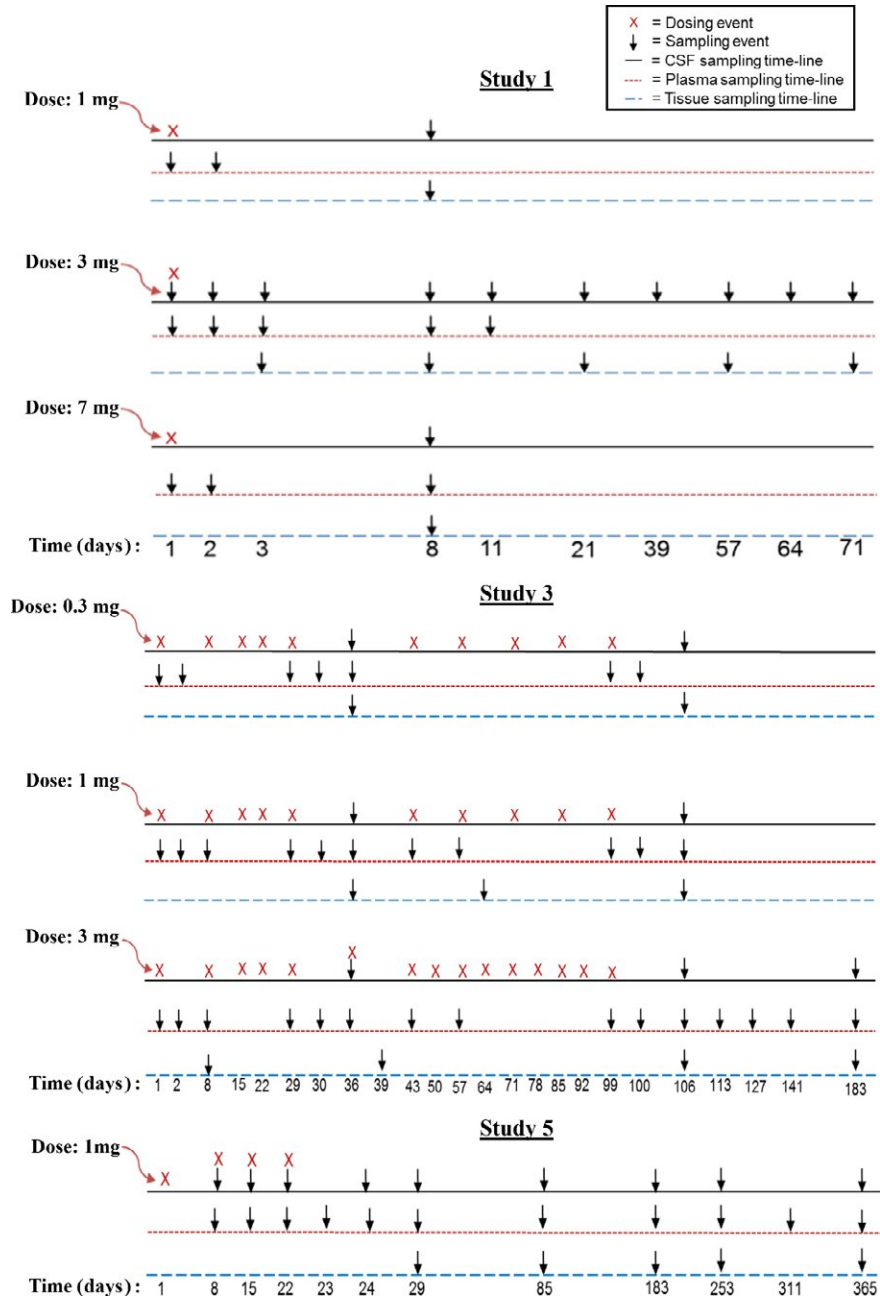


**Figure 1** Dosing and sampling schedule in days for studies 1 (single dose study), 3 (multiple dose study), and 5 (multiple dose study). CSF, cerebrospinal fluid.

considered as a unified “brain” lumped tissue for model simplicity and to avoid over-parameterization; (ii) drug concentration in the brain compartment was assumed to be equal to the median concentration of the lumped compartments, in a physiological context, this unified “brain” compartment was considered to be bathed in the CSF, although CSF does not bathe the interior of the brain; (iii) provided that the drug has high accumulation and retention time in the brain, accounting for the rapid turnover of CSF, an additional compartment (compartment #5) was included in the model, wherein the drug can diffuse between the unified brain compartment and

the additional “deep brain” compartment. This “deep brain” compartment accounted for potential residual brain tissues that were not evaluated for drug concentration during sample analysis. In addition, incorporating this compartment in the model resulted in a significantly lower interindividual variability (IIV) in model parameters and allowed for successful parameter estimation. (iv) Due to its anatomic and physiological important function as a relay station to facilitate travel of neuronal information between forebrain and cerebellum, pons was considered an important tissue in the context of SMA. Hence, pons was considered a separate region from

the cortex and deep brain structures during the modeling effort. An attempt was also made to characterize nusinersen PK in pons in the context of SMA. Drug concentration was assumed to be equal between pons and the brain stem (in each case, the drug concentration was only measured in one of these two tissues). These assumptions were expected to only negligibly affect the validity of the model.

The model was parameterized using first-order rate constants to describe nusinersen distribution among CSF (site of injection), CNS, and various tissues (see **Figure 2**). Based on the current literature information for large molecules, nusinersen was postulated to exit the CNS unidirectionally from the CSF into plasma.<sup>20,21</sup> Degradation of the drug within the brain tissue is plausible, and this was evaluated during initial model-building efforts. However, due to the extremely long terminal elimination half-life of the drug in the CSF (~4–6 months),<sup>18</sup> and sparseness of time-staggered data, reliable estimation of this degradation parameter was not feasible using PK data available at the time of modeling. Parameter estimation was performed using the first-order conditional estimation method with interaction. Exponential IIV was evaluated on each parameter in a step-wise manner with the assumption of log-normal distribution of all PK parameters. A drop of at least 3.84 points ( $P < 0.05$ ) in the OFV with each additional parameter was considered as a statistical criterion for parameter inclusion. Residual unexplained variability (RUV) was included as a proportional error in the model. The GOF plots and VPCs were used for model evaluation. The VPCs were performed using MatVPC.<sup>22</sup> The

robustness of the model was evaluated by performing a nonparametric bootstrap ( $n = 500$ ). The median and 95% confidence intervals (CIs) of the bootstrap were calculated for each parameter and compared to the parameter estimates of the original dataset.

### Nonhuman primate to clinical scaling

Body weight-based allometric scaling was implemented to scale all rate constants included in the final model. In 2011, Mahmood<sup>23</sup> estimated an allometric exponent range of ~0.5–0.83 for clearance, and a range of 0.31–0.76 for volume of distribution for oligonucleotides. Mahmood<sup>23</sup> concluded that the use of a fixed exponent for allometric scaling of PK parameters could lead to highly erroneous predictions. Similarly, Callies *et al.*<sup>24</sup> used an allometric scaling exponent of 1 for clearance of second-generation ASO, indicating that such deviation for large molecules compared to the typically used exponent range of 0.67–0.75 for small molecules is to be expected due to the inherent differences in mechanism of clearance between small and large molecules. Additionally, scaling exponents of 0.922 and 1.19 for clearance and volume has also been reported for scaling of second-generation ASO from monkeys to humans.<sup>25</sup> Accordingly, the typically reported allometric scaling exponents for the first-order rate constants of -0.25, as well as -0.5 and -0.08 were methodically evaluated in the current work using Eq. 1.<sup>26</sup> It is to be noted that no model-fitting or parameter estimation was attempted during the scaling of the NHP model because no clinical tissue PK data was

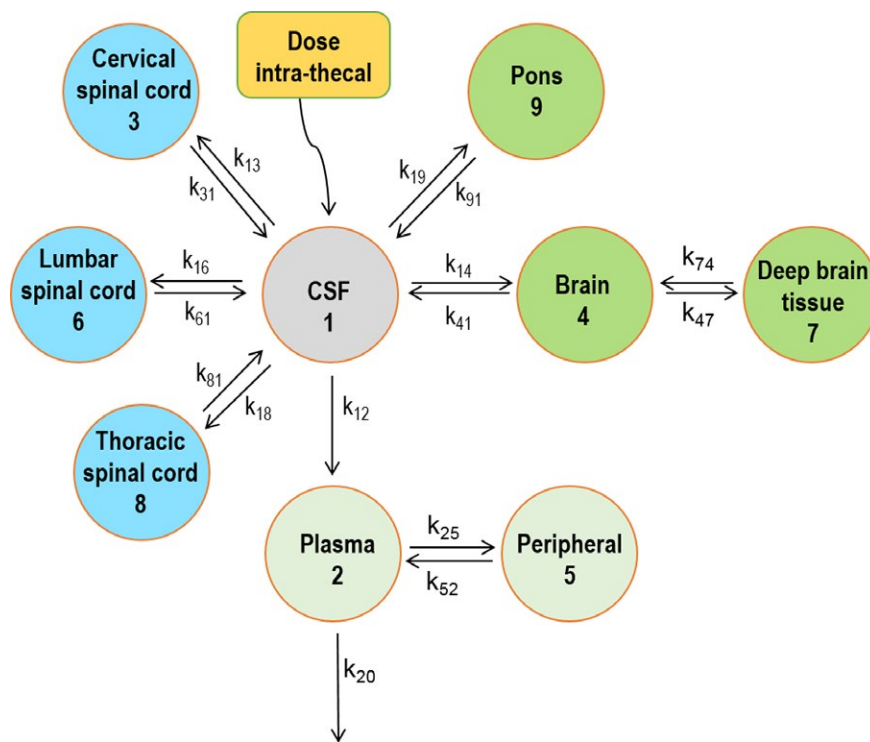


**Figure 2** Illustration of the final nonhuman primate (NHP) population pharmacokinetic model. The model consists of nine compartments in total, namely cerebrospinal fluid (CSF), plasma, cervical spinal cord, brain, deep brain tissue, lumbar spinal cord, thoracic spinal cord, and a peripheral distribution compartment. Nusinersen is administered as an i.t. bolus dose into the CSF compartment. The  $k_{ij}$  represents the first-order rate constant describing the distribution of the drug from compartment  $i$  to compartment  $j$ .

available. The clinical data from CSF and plasma samples were only used for model evaluation, and the scaled-up model simulations were overlaid with the clinical data for visual comparison.

$$\text{Parameter}_{\text{pediatric}} = \text{Estimated parameter}_{\text{NHP}} * \left( \frac{\text{BW}_{\text{pediatric}}}{\text{Median BW}_{\text{NHP}}} \right)^{\text{Exponent}} \quad (1)$$

Provided that there are low levels of endogenous proteins in CSF for drug-protein binding, and that the physiological volume of CSF only increases approximately up to 2 years after birth,<sup>27</sup> the CSF volume of distribution ( $V_d$ ) was fixed to pediatric age-range based on literature reported<sup>28</sup>

physiological cutoff values. The BW-based allometric scaling was implemented for the remaining NHP estimated  $V_d$  and exponent values of 1 and 1.19 were evaluated. Simulations ( $n = 1,000$ ) using pediatric demographics and clinical trial dosing information were performed using the allometric scaled parameters. Because the NHP model was not fitted to pediatric data, it was not possible to determine the IIV in pediatric patients. Thus, the IIV estimates from the NHP PK model fitting were fixed and subsequently used for pediatric simulations. As a result, only those NHP PK model parameters (see **Table 1** for model parameters with associated IIV) that had an IIV term associated with them were correspondingly varied between pediatric patients during NHP-to-pediatric simulations. To evaluate the predictive

**Table 1** Final population parameter estimates and bootstrap results of the NHP population pharmacokinetic model.  $V_i$  denotes the volume of distribution of compartment  $i$  (**Figure 2** illustrates the compartment numbers and the structure of the model).  $k_{ij}$  represents the first-order rate constant describing the distribution of the drug from compartment  $i$  to compartment  $j$ .

Parameters	Description (unit)	Population parameter estimates [bootstrap median (95% CI)]	IIV (%) [bootstrap median (95% CI)]
$V_1$	CSF volume (mL)	13.6 [16.4 (14.1–109.2)]	92.4 [92.3 (77.1–498.6)]
$V_2$	Plasma volume (mL)	937 [790 (394–877)]	91.2 [115.6 (59.5–177)]
$V_3$	Cervical spinal cord (mL)	1.91 [2.48 (1.98–8.09)]	–
$V_4$	Brain volume (mL)	53.8 [54.3 (2.5–62)]	–
$V_6$	Lumbar spinal cord volume (mL)	1.08 [1.38 (1.12–6.35)]	–
$V_8$	Thoracic spinal cord volume (mL)	1.52 [1.67 (0.73–9.21)]	–
$V_9$	Pons volume (mL)	2.11 [2.2 (1.29–13.65)]	–
$k_{13}$	CSF to cervical spinal cord (1/hour)	0.00171 [0.00143 (0.001–0.0059)]	67.3 [52.8 (23.9–75.8)]
$k_{31}$	Cervical spinal cord to CSF (1/hour)	0.0001 [0.0001 (0.0001–0.0005)]	–
$k_{14}$	CSF to brain (1/hour)	0.006 [0.006 (0.0059–0.111)]	368.8 [119.3 (75.2–139)]
$k_{41}$	Brain to CSF (1/hour)	0.0004 [0.00056 (0.0004–0.0076)]	39.5 [26.6 (18.9–88.1)]
$k_{12}$	CSF to plasma (1/hour)	0.0891 [0.0921 (0.0838–0.1269)]	114.0 [107 (8.7–132.6)]
$k_{20}$	Plasma to out of body (1/hour)	0.206 [0.218 (0.189–0.649)]	64.9 [ 55.8 (14.9–131.6)]
$k_{25}$	Plasma to periphery (1/hour)	0.00818 [0.00824 (0.00706–0.02217)]	–
$k_{52}$	Periphery to plasma (1/hour)	0.0001 [0.0001 (0.0001–0.0036)]	–
$k_{16}$	CSF to lumbar spinal cord (1/hour)	0.00286 [0.00236 (0.00181–0.00734)]	35.2 [13 (4.6–44.2)]
$k_{61}$	Lumbar spinal cord to CSF (1/hour)	0.0003 [0.00033 (0.00024–0.00038)]	–
$k_{47}$	Brain to deep tissue (1/hour)	0.00257 [0.00231 (0.00193–0.0126)]	–
$k_{74}$	Deep tissue to brain (1/hour)	0.0001 [0.0001 (6.07E-05–0.000285)]	–
$k_{18}$	CSF to thoracic spinal cord (1/hour)	0.0021 [0.0018 (0.0006–0.0053)]	52.9 [45.1 (28.9–91.1)]
$k_{81}$	Thoracic spinal cord to CSF (1/hour)	0.00045 [0.00042 (0.00003–0.000458)]	35.9 [14 (2.8–248.8)]
$k_{19}$	CSF to pons (1/hour)	0.00157 [0.00095 (0.00031–0.0041)]	80.9 [85.3 (37.3–156.3)]
$k_{91}$	Pons to CSF (1/hour)	0.0002 [0.00021 (0.0002–0.0007)]	53.9 [29.4 (3.5–31.4)]
Residual unexplained variability (%) [Bootstrap median (95% CI)]			
CSF		71.4 [64.6 (50.3–73.6)]	–
Plasma		41.2 [39.2 (30.4–56.7)]	–
Cervical spinal cord		10.1 [10 (1.7–10.1)]	–
Brain		177 [154 (46–173)]	–
Lumbar spinal cord		31.2 [36.7 (16.7–62)]	–
Thoracic spinal cord		2.39 [2.39 (1.94–2.39)]	–
Pons		1.03 [1.03 (0.98–1.03)]	–

CI, confidence interval; CSF, cerebrospinal fluid; IIV, interindividual variability.

performance of the model, at each time point, the fold-difference between the simulation's median and the median of the clinical data was calculated.

### Sensitivity analysis

Global sensitivity analysis (Sobol) was conducted using MATLAB<sup>29</sup> to identify the parameters that drive the NHP PopPK model dynamics and particularly the maximum drug concentration ( $C_{\max}$ ) of nusinersen in each compartment of the NHP model. The criterion for evaluating the impact of each parameter on NHP PopPK model behavior was the change in  $C_{\max}$  of a particular compartment. More specifically, a large change in  $C_{\max}$  upon modifying a parameter indicates that the latter plays a pivotal role in shaping model behavior, whereas a small change in  $C_{\max}$  upon modifying a parameter implies that this parameter does not significantly impact model behavior.

Collectively, six sensitivity analyses were conducted, one for each of the following compartments: (i) plasma, (ii) cervical spinal cord, (iii) lumbar spinal cord, (iv) thoracic spinal cord, (v) pons, and (vi) brain. The CSF was not included in this analysis as it is the dosing compartment. In addition, the deep brain tissue as well as the peripheral compartment was excluded from this analysis as there were no observations for these compartments. Sensitivity analysis was performed as follows<sup>29</sup>: the Multi-Objective Evolutionary Algorithm framework was used to generate 340,000 random values for each parameter (5,440,000 in total). These values were within  $\pm 30\%$  of the nominal parameter values estimated by NONMEM (Table 1). The NHP PopPK model was simulated 340,000 times in MATLAB, using these random parameter values, and the  $C_{\max}$  of each compartment was calculated. The outcome of the simulations was subsequently inserted back to the Multi-Objective Evolutionary Algorithm framework to calculate the global sensitivity indices. In these simulations, neither IIV nor RUV were considered, as the goal was to simply monitor the absolute changes in  $C_{\max}$  upon modifying the parameter values. Accounting for IIV and RUV would not allow for determining the change in  $C_{\max}$  that was caused solely by the parameter modification.

To illustrate our sensitivity analyses findings, simulations of the NHP PopPK model were carried out in MATLAB. In each simulation, a 10% increase in one of the parameter values was applied and the PK profiles for each compartment were calculated. These PK profiles were then compared with the PK profile from the simulations with the nominal parameter values.

## RESULTS

### NHP PopPK analysis

A two-compartment i.v. plasma concentration NHP PopPK model was selected, based on the lowest OFV, GOF plots, and VPCs for further model expansion. The final NHP PopPK model that was built with i.t. dosing data consisted of nine compartments, namely CSF, plasma, brain, deep brain tissue, cervical spinal cord, thoracic spinal cord, lumbar spinal cord, pons, and a peripheral plasma compartment (Figure 2). The NONMEM code for the model is provided in Data S2. The IIV was found to be statistically significant on all rate constants associated with the CSF compartment and plasma elimination rate constants.

In addition, IIV was included on CSF and plasma  $V_d$ . The final NHP PK parameter estimates are shown in Table 1. The results of the bootstrap analysis (Table 1) show that the majority of the estimates fall within the 95th CI of the bootstrap estimates, thereby demonstrating the validity of the estimates. However, few parameters were slightly outside of the 95th CI of the bootstrap estimates ( $V_1$ ,  $V_2$ ,  $V_3$ ,  $V_6$ , IIV<sub>k14</sub>, IIV<sub>k91</sub>, and RUV<sub>Brain</sub>). In general, this discrepancy between the model and the bootstrap estimates could be attributed to the instability of the model and the relative low number of bootstrap samples ( $n = 500$ ), which could not be increased due to the long time needed for each sample (~5 days). In particular, this discrepancy might stem from the sparse and, thus, very variable data that could give rise to high IIV estimates (e.g., IIV<sub>k14</sub> and IIV<sub>k91</sub>), or to the fact that different subcompartments were lumped together and only their median concentrations were considered, and, thus,  $V_{\text{Brain}}$  could not be described perfectly. Nevertheless, an exhaustive search of different model structures (Thetas and Etas) demonstrated that the presented model provides the best balance of model complexity and observations fitting. An indication of this is that some of the model estimates (CSF volume ( $V_1$ ); total spinal cord volume ( $V_3 + V_6 + V_8$ )) are comparable to literature reported values.<sup>30-34</sup> The individual data fit (Figure 3) as well as the VPC plots (Figure 4) demonstrated an overall good agreement between model predictions and observations. It should be noted that after stratifying on study ( $n = 3$ ), dose ( $n = 4$ ), and compartment of interest ( $n = 7$ ), a total of 49 VPC plots were generated. Figure 4 shows representative VPC plots for the compartments CSF and plasma, as generated by MatVPC.

As shown in Figure 3, the drug concentration in the brain compartment was not predicted with high accuracy. This was also reflected in the significantly high estimated RUV on the brain compartment. The difference between the predictions and observations could be attributed to the fact that the various brain subcompartments were lumped together and only the median value of their concentrations was considered. However, as mentioned earlier, expanding the model further to include the various brain subcompartments led to overparameterization and model instability. Finally, it should be noted that instead of staggered sampling collection time points, the majority of the available PK data were sampled at the same time points across studies (as the majority of monkeys were euthanized at the same time after dosing) thereby providing a limited concentration-time profile, which deemed the precise parameter estimation challenging.

It is important to stress that our analysis indicated that the rate constants describing the distribution of drug out of CSF was ~4-fold (between CSF and thoracic spinal cord) to 20-fold (between CSF and brain) larger than their respective rate constants describing drug distribution back to CSF. The low distribution back to the CSF is in line with the long half-life of nusinersen, whose mean terminal elimination half-life is estimated to be 135 to 177 days in CSF, and 63 to 87 days in plasma.<sup>18</sup>

### NHP to clinical scaling

The BW-based allometric scaling was implemented to scale the NHP PK parameters to pediatrics in order to

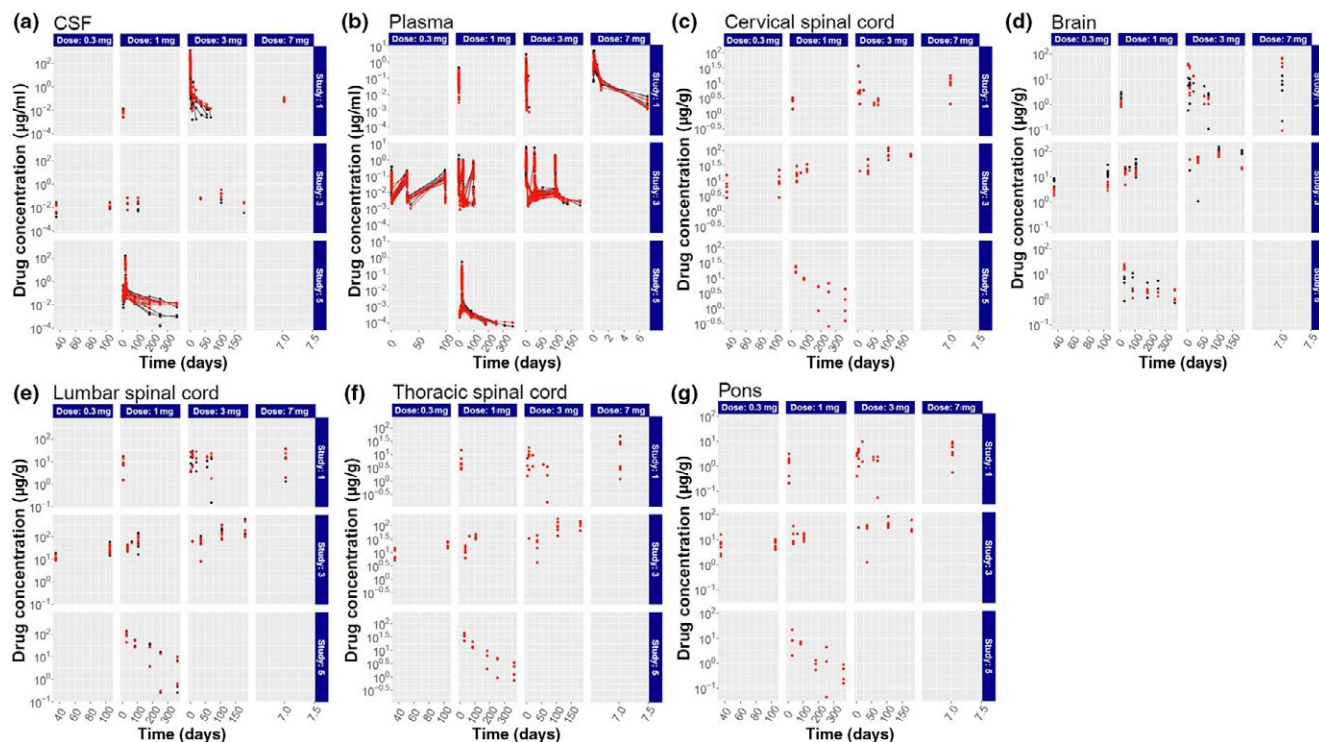


**Figure 3** Final model predictions (red), along with the corresponding observations from nonhuman primate (black), for the compartments, cerebrospinal fluid (CSF) (a), plasma (b), cervical spinal cord (c), brain (d), lumbar spinal cord (e), thoracic spinal cord (f), and pons (g). Within each subplot (a-g), the four different columns correspond to four different doses (0.3, 1, 3, and 7 mg) whereas the three different rows represent three different studies (1, 3, and 5). For dosing schedule information please see **Figure 1**.

predict pediatric nusinersen concentrations in different tissues, CSF, and plasma. Among the evaluated allometric scaling parameters, an exponent value of  $-0.08$  for the rate constants and an exponent value of  $1$  for  $V_d$  provided the best agreement between the simulation median and the clinical data. The NONMEM code for the simulations is provided in **Data S1**. Plots overlaying the median profiles of the simulations and the observations for CSF and plasma from pediatrics are shown in **Figure 5**. The analysts were blinded to the clinical observations shown in **Figure 5** during model development and the data were made available only after the simulations were executed. The clinical observations were exclusively utilized for model evaluation by overlaying the simulations with the observed data. At a dose of  $1$  mg, 100% of the CSF observations were within a 2-fold difference from the simulations whereas at a dose of  $9$  mg, only 20.7% of the CSF observations were within a 2-fold difference. Regarding the plasma concentrations, at a dose of  $1$  mg, 42.9% of the observations were within a 2-fold difference from the simulations and at a dose of  $9$  mg, 67.6% of the observations were within a 2-fold difference.

### Sensitivity analysis

Global sensitivity analysis demonstrated that only two processes play a dominant role in the determination of  $C_{max}$  value in each compartment: (i) the first-order rate constant describing the rate of drug exchange between CSF and the respective compartment ( $k_{13}$ ,  $k_{14}$ ,  $k_{16}$ ,  $k_{18}$ , and  $k_{19}$  for

cervical spinal cord, brain, lumbar spinal cord, thoracic spinal cord, and pons, respectively), and (ii) the first-order rate constant describing the rate of drug distribution from CSF to plasma ( $k_{12}$ ) and from plasma to out of the body ( $k_{20}$ ). The value of these two parameters for each tissue shapes the  $C_{max}$  of nusinersen in the respective tissue and modifying this value could be used to regulate the  $C_{max}$  of the drug. **Figure 6** describes the sensitivity indices of each parameter for the six compartments that were explored.

Simulations based on the NHP PopPK model upon increasing each parameter value by 10% were performed in MATLAB to cross validate the sensitivity analysis findings (**Figure 6**). In consistency with the Sobolj sensitivity analyses, the simulations showed that a +10% perturbation in one of the parameters  $k_{20}$ ,  $k_{13}$ ,  $k_{14}$ ,  $k_{16}$ ,  $k_{18}$ ,  $k_{19}$ , and  $k_{12}$  results in a sizable change in the PK profile and consequently in the  $C_{max}$  of the corresponding compartment. In contrast, increasing any other parameter by 10% resulted in PK profiles that nearly paralleled the PK profile from the simulations with the nominal values (nominal values shown in **Table 1**).

### DISCUSSION

The aim of the present study was to develop a translational NHP PopPK model of nusinersen using NHP PK data and subsequent model scale-up to predict the PK in pediatric patients with SMA. This would aid in characterizing nusinersen PK at the site(s) of central action in order for optimizing clinical trial design, expediting nusinersen's

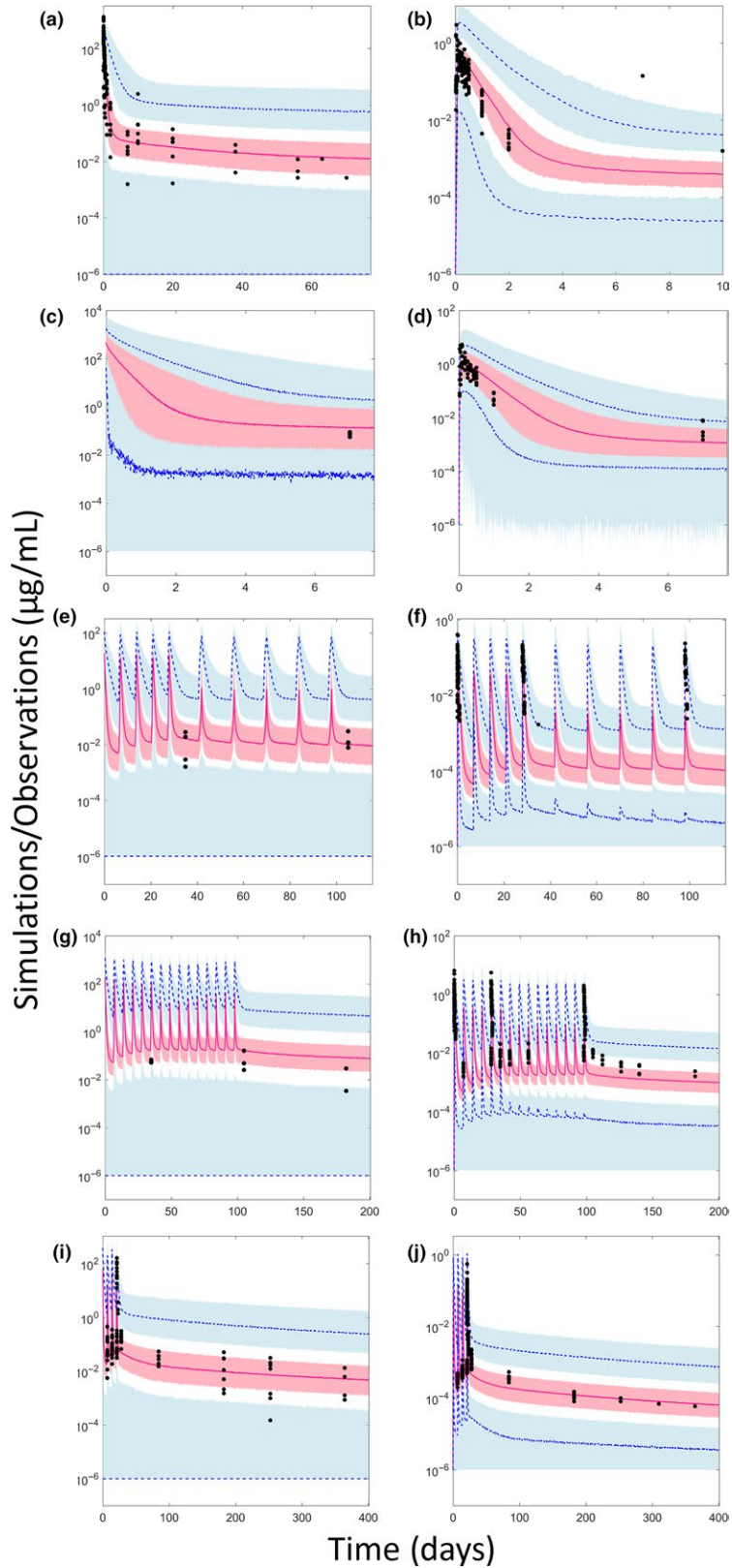
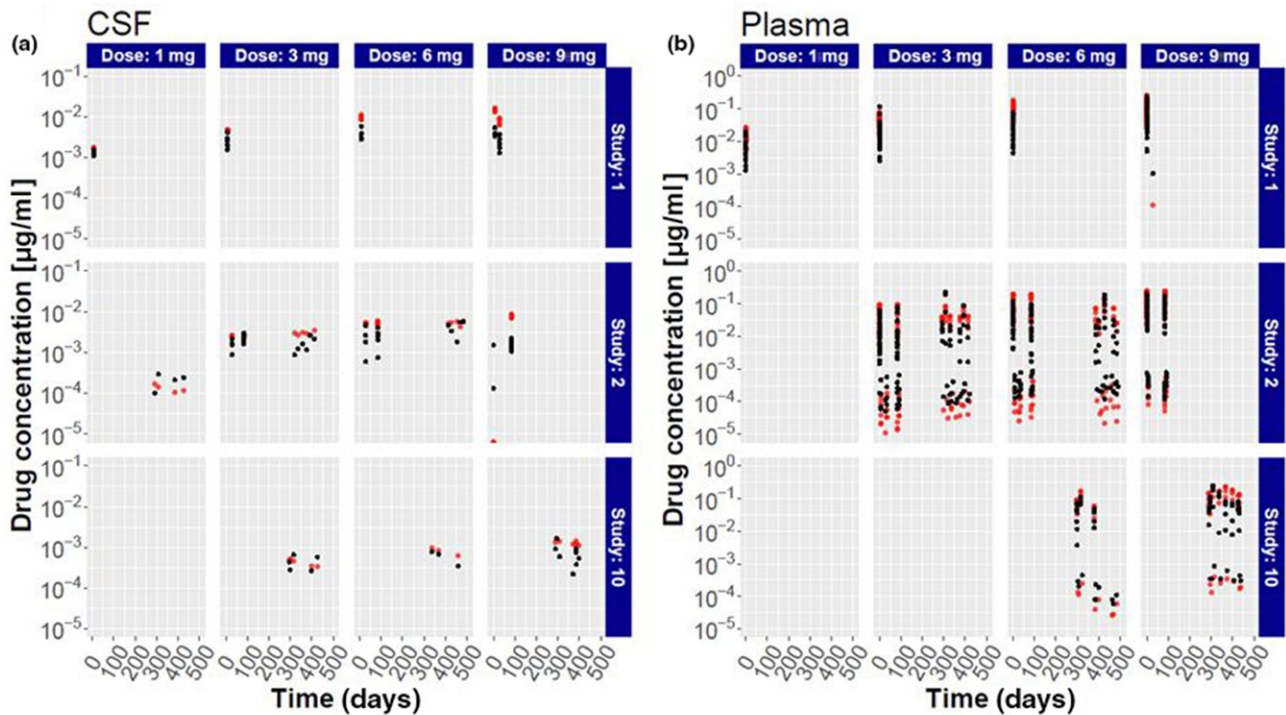


**Figure 4** Representative (out of 49 in total) visual predictive checks for the compartments cerebrospinal fluid (CSF) (a, c, e, g, i) and plasma (b, d, f, h, j) for study 1 and dose 3 mg (a, b), study 1 and dose 7 mg (c, d), study 3 and dose 0.3 mg (e, f), study 3 and dose 3 mg (g, h), and study 5 and dose 1 mg (i, j). Black dots represent the observations from nonhuman primates, blue lines show the median of the 5th and 95th simulated percentiles, and red lines represent the median of the 50th simulated percentiles. Shaded areas correspond to the 90% confidence intervals.



(c)

Dose (mg)	<i>n</i> (total)	% of over-prediction < 2-fold	% of over-prediction within 2-3 fold	% of over-prediction > 3-fold
<b>CSF</b>				
1	9	100	0	0
3	25	76.0	20.0	4.0
6	24	58.3	16.7	25.0
9	29	20.7	20.7	58.6
<b>Plasma</b>				
1	28	42.9	32.1	25.0
3	150	56.7	24.7	18.6
6	170	56.5	18.2	25.3
9	219	67.6	18.3	14.1

**Figure 5** (a, b) Simulations ( $n = 1000$ , red) of phase I clinical pediatric data (black) for the compartments cerebrospinal fluid (CSF) (a) and plasma (b). The results were generated upon scaling the model from nonhuman primates to pediatrics by implementing body weight-based allometric scaling. An exponent value of  $-0.08$  and  $1$  was used for rate constants and volumes ( $V_2$ ,  $V_3$ ,  $V_4$ ,  $V_6$ ,  $V_8$ , and  $V_9$ ), respectively. The CSF volume was fixed to pediatric age-based physiological cutoff values (120 mL for ages  $<0.25$  years old, 130 mL for ages within 0.25–0.5 years old, 135 mL for ages within 0.5–1 years old, 140 mL for ages within 1–2 years old, and 150 mL for ages  $>2$  years old). Within each subplot (a, b), the four different columns correspond to four different doses (1, 3, 6, and 9 mg), whereas the three different rows represent different studies (1, 2, and 10). (c) Percent fold difference between predicted and observed clinical concentrations as shown in Figure 5a,b;  $n$  indicates total number of observations from pediatrics.

development, and, more importantly, delivering a therapeutically beneficial treatment for patients with SMA.

NHPs and clinical data of nusinersen were used in this work. In an initial analysis, by using i.v. dosing data, a two-compartment model was found to accurately describe the plasma PK of nusinersen. Once the plasma PK was adequately characterized, the analysis was focused on

expanding the model to account for nusinersen PK in the CSF, spinal cord, and brain following i.t. administration. The CSF is produced in the choroid plexus and it bathes the brain and spinal cord.<sup>35</sup> Hence, the different subcompartments of the spinal cord and brain were modeled as mammillary compartments connected to the CSF. The subcompartments within a particular tissue were not linked to

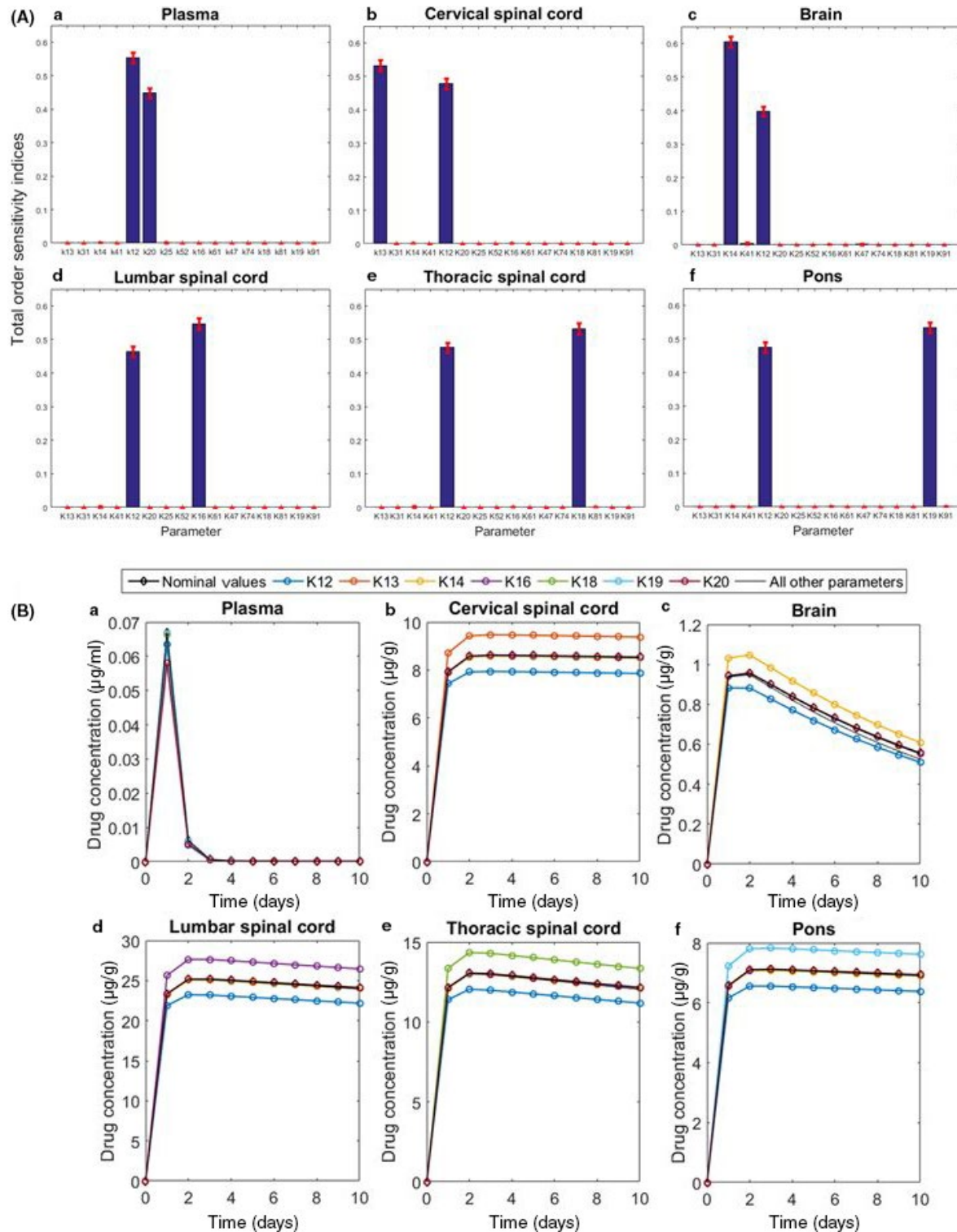


**Figure 6 A:** Total order sensitivity indices from Sobol Sensitivity analysis for the compartments plasma (a), cervical spinal cord (b), brain (c), lumbar spinal cord (d), thoracic spinal cord (e), and pons (f). The error bars shown in red correspond to the confidence intervals (CIs) as calculated by bootstrapping ( $CI_{95\%} = \text{sensitivity index} \pm \text{bootstrap CI}$ ). **B:** Simulations of drug concentrations (1 mg dose) in nonhuman primates for the compartments plasma (a), cervical spinal cord (b), brain (c), lumbar spinal cord (d), thoracic spinal cord (e), and pons (f). In these simulations, the estimated parameter values (black line with diamond marker) as well as the estimated parameter values with one parameter value being increased by 10% were simulated. Solid black lines correspond to simulations wherein a 10% increase of a parameter did not affect model dynamics appreciably. Colored lines with a circle marker correspond to simulations wherein a 10% increase in a parameter had high impact on the model behavior.

each other because to our knowledge there is no clear evidence that the drug can traverse freely between the sub-compartments. In the interest of modeling simplicity and to avoid overparameterization, the potential degradation of the drug within the tissue was not included in the final model. Therefore, the only mode of systemic drug elimination was via the plasma compartment.

Following i.t. dosing, the drug distributes immediately into the spinal cord and brain tissues, as evidenced by the rapid decrease of nusinersen concentrations in the CSF. Furthermore, the drug concentration in these tissues remains significantly high for a prolonged period of time. This is reflected by the ~4–20-fold difference between the rate of drug distribution from CSF to cervical spinal cord ( $k_{13}$ ), brain ( $k_{14}$ ), lumbar spinal cord ( $k_{16}$ ), thoracic spinal cord ( $k_{18}$ ), and pons ( $k_{19}$ ) and the rate of drug distributing back from these compartments to CSF ( $k_{31}$ ,  $k_{41}$ ,  $k_{61}$ ,  $k_{81}$ , and  $k_{91}$ ). As such, the drug exhibits a long tissue half-life (~4–6 months). Moreover, the parameter estimates for the rate constants suggest differences in the rate of drug uptake between the three spinal cord subcompartments. The rate of drug uptake from CSF to lumbar region ( $k_{16}$ ,  $0.0029\text{ d}^{-1}$ ) is almost twice as fast as the rates of drug uptake from CSF to thoracic ( $k_{18}$ ,  $0.0021\text{ d}^{-1}$ ) or cervical ( $k_{13}$ ,  $0.0017\text{ d}^{-1}$ ) spinal cord regions. This is possibly related to the site of drug administration, which is the lower spinal cord near the lumbar region. Therefore, a higher concentration gradient would exist in the proximity of the lumbar spinal cord resulting in greater drug diffusion in this region compared to the more remote regions of the spinal cord.

Global sensitivity analysis demonstrated that the rate constants associated with drug distribution from CSF to its interacting compartments were highly influential and sensitive, thus indicating that a small imprecision in the estimation of these parameters can lead to erroneous model predictions. Simulations in MATLAB, wherein each parameter was perturbed, validated the outcome of the sensitivity analysis.

Typically, pediatric drug development begins with scaling-up of a preclinical PK model to predict PK in adult patients and later followed by scaling-down the adult human model to predict PK in pediatric patients. However, there is no adult patient PK data available due to the low life expectancy of patients with SMA (<2 years in type I SMA<sup>36</sup>), the NHP model developed in the current work was scaled directly to predict pediatric drug concentrations. Considering that CSF volume increases during the first 2 years after birth, this information was incorporated into the scaling and the physiological age-related volumes of pediatrics were used.<sup>37</sup> The BW-based allometric scaling of rate constants (exponent value of  $-0.08$ ) and  $V_d$  (exponent value of 1) best captured the pediatric CSF and plasma drug concentrations across all studies and doses. The majority of model predictions were within threefold range of the observations.

In conclusion, a semimechanistic, PopPK model for nusinersen, a second-generation ASO with linear clearance, was successfully developed. The model predicted nusinersen PK in NHP with reasonable precision across

all studies and all evaluated doses. Although in some instances the individual model predictions were not consistent with the observations, the main goal of this study was to capture the central tendency of the model and not strictly the individual behavior.<sup>38</sup> Upon allometric scaling, the NHP model was able to predict drug PK for CSF and plasma in pediatric patients with SMA within acceptable limits. The developed model can be utilized as a means for guiding the design and optimization of future clinical trials of ASOs.

### Supporting Information

Supplementary information accompanies this paper on the *CPT: Pharmacometrics & Systems Pharmacology* website. ([www.psp-journal.com](http://www.psp-journal.com))

**Data S1.** NONMEM code for pediatric simulations.

**Data S2.** NONMEM code for estimation of the NHP model parameter values.

**Acknowledgments.** This analysis was supported by Biogen. K.B. and P.G. contributed equally to the analysis.

**Funding.** This analysis was supported by Biogen.

**Conflict of Interest.** D.N., Y.W., and S.H. are employees of Ionis Pharmaceuticals and R.F. was with Ionis at the time of analysis, I.N. is an employee of Biogen, W.Y. and M.R. were employees of Biogen at the time of analysis.

**Author Contributions.** K.B., P.G., and M.N.T. wrote the manuscript. M.N.T., L.J.L., S.S., W.Y., I.N., and M.R. designed the research. K.B., P.G., and M.N.T. performed the research. K.B., P.G., and M.N.T. analyzed the data. D.A.N., Y.W., S.H., and R.F. contributed new reagents/analytical tools.

1. D'Amico, A., Mercuri, E., Tiziano, F.D. & Bertini, E. Spinal muscular atrophy. *Orphanet. J. Rare Dis.* **6**, 71 (2011).
2. Lunn, M.R. & Wang, C.H. Spinal muscular atrophy. *Lancet* **371**, 2120–2133 (2008).
3. Talbot, K. & Davies, K.E. Spinal muscular atrophy. *Semin. Neurol.* **21**, 189–197 (2001).
4. Castro, D. & Iannaccone, S.T. Spinal muscular atrophy: therapeutic strategies. *Curr. Treat. Options Neurol.* **16**, 316 (2014).
5. Sugarman, E.A. et al. Pan-ethnic carrier screening and prenatal diagnosis for spinal muscular atrophy: clinical laboratory analysis of >72,400 specimens. *Eur. J. Hum. Genet.* **20**, 27–32 (2012).
6. Crawford, T.O. & Pardo, C.A. The neurobiology of childhood spinal muscular atrophy. *Neurobiol. Dis.* **3**, 97–110 (1996).
7. Kolb, S.J. & Kissel, J.T. Spinal muscular atrophy: a timely review. *Arch. Neurol.* **68**, 979–984 (2011).
8. Lorson, C.L., Hahnen, E., Androphy, E.J. & Wirth, B. A single nucleotide in the SMN gene regulates splicing and is responsible for spinal muscular atrophy. *Proc. Natl. Acad. Sci. USA* **96**, 6307–6311 (1999).
9. Naryshkin, N.A. et al. Motor neuron disease. SMN2 splicing modifiers improve motor function and longevity in mice with spinal muscular atrophy. *Science* **345**, 688–693 (2014).
10. d'Ydewalle, C. & Sumner, C.J. Spinal muscular atrophy therapeutics: where do we stand? *Neurother. J. Am. Soc. Exp. Neurother.* **12**, 303–316 (2015).
11. Farrar, M.A. & Kiernan, M.C. The genetics of spinal muscular atrophy: progress and challenges. *Neurother. J. Am. Soc. Exp. Neurother.* **12**, 290–302 (2015).
12. Nizzardo, M. et al. Beta-lactam antibiotic offers neuroprotection in a spinal muscular atrophy model by multiple mechanisms: Experimental Neurology 2011; 229: 214–225. *Ann. Neurosci.* **18**, 156–157 (2011).

13. Ebert, A.D. *et al.* Induced pluripotent stem cells from a spinal muscular atrophy patient. *Nature* **457**, 277–280 (2009).
14. O'Hare, E. & Young, P.J. Childhood spinal muscular atrophy and stem cell research: is cellular replacement therapy the answer? (Review). *Mol. Med. Rep.* **2**, 3–5 (2009).
15. Mulcahy, P.J. *et al.* Gene therapy: a promising approach to treating spinal muscular atrophy. *Hum. Gene Ther.* **25**, 575–586 (2014).
16. Passini, M.A. *et al.* Antisense oligonucleotides delivered to the mouse CNS ameliorate symptoms of severe spinal muscular atrophy. *Sci. Transl. Med.* **3**, 72ra18 (2011).
17. Zanetta, C. *et al.* Molecular, genetic and stem cell-mediated therapeutic strategies for spinal muscular atrophy (SMA). *J. Cell. Mol. Med.* **18**, 187–196 (2014).
18. SPIRANZA US Prescribing Information [Internet]. Accessed 2 June 2017. <<https://www.spinraza.com/PI>>
19. Yu, R.Z., Baker, B., Chappell, A., Geary, R.S., Cheung, E. & Levin, A.A. Development of an ultrasensitive noncompetitive hybridization-ligation enzyme-linked immunosorbent assay for the determination of phosphorothioate oligodeoxynucleotide in plasma. *Anal. Biochem.* **304**, 19–25 (2002).
20. Pardridge, W.M. The blood-brain barrier: bottleneck in brain drug development. *NeuroRx* **2**, 3–14 (2005).
21. Geary, R.S., Norris, D., Yu, R.Z. & Bennett, F. Pharmacokinetics, biodistribution and cell uptake of antisense oligonucleotides. *Adv. Drug Deliv. Rev.* **87**, 46–51 (2015).
22. Biliouris, K., Lavielle, M. & Trame, M.N. MatVPC: a user-friendly Matlab-based tool for the simulation and evaluation of systems pharmacology models. *CPT Pharmacometrics Syst. Pharmacol.* **4**, 547–557 (2015).
23. Mahmood, I. Pharmacokinetic allometric scaling of oligonucleotides. *Nucleic Acid Ther.* **21**, 315–321 (2011).
24. Callies, S. *et al.* Integrated analysis of preclinical data to support the design of the first in man study of LY2181308, a second generation antisense oligonucleotide. *Br. J. Clin. Pharmacol.* **71**, 416–428 (2011).
25. Callies, S. *et al.* Modelling pharmacokinetic and pharmacodynamic properties of second generation antisense-oligonucleotides (ASOs) [Internet]. Denmark, Kobenhavn: PAGE Meeting. <[https://www.page-meeting.org/pdf\\_assets/6497-poster\\_ASOS\\_Page13\\_June\\_2007\\_Copenhagen.pdf](https://www.page-meeting.org/pdf_assets/6497-poster_ASOS_Page13_June_2007_Copenhagen.pdf)> (2007). Accessed 6 February 2017.
26. Anderson, B.J. & Holford, N.H.G. Mechanism-based concepts of size and maturity in pharmacokinetics. *Annu. Rev. Pharmacol. Toxicol.* **48**, 303–332 (2008).
27. Matsuzawa, J. *et al.* Age-related volumetric changes of brain gray and white matter in healthy infants and children. *Cereb. Cortex* **11**, 335–342 (2001).
28. Altman, P.L. & Dittmer, D.S. Biology data book. AMRL-TR-64-100. AMRL TR. 1–631 (1964).
29. Zhang, X.-Y., Trame, M.N., Lesko, L.J. & Schmidt, S. Sobol sensitivity analysis: a tool to guide the development and evaluation of systems pharmacology models. *CPT Pharmacometrics Syst. Pharmacol.* **4**, 69–79 (2015).
30. Artu, A. Spinal cerebrospinal fluid chemistry and physiology. In *Preclinical Safety Evaluation for Spinal Drugs. Spinal Drug Delivery* (ed. Yaksh, T.) 417–437 (Elsevier Science BV., Amsterdam, 1999).
31. Oh, S.A., Kang, M.K., Kim, S.K. & Yea, J.W. Comparison of IMRT and VMAT techniques in spine stereotactic radiosurgery with international spine radio-surgery consortium consensus guidelines. *Progress Med. Phys.* **24**, 145–153 (2013).
32. Burish, M.J., Peebles, J.K., Baldwin, M.K., Tavares, L., Kaas, J.H. & Herculano-Houzel, S. Cellular scaling rules for primate spinal cords. *Brain Behav. Evol.* **76**, 45–59 (2010).
33. Afifi, A.K. & Bergman, R.A. *Functional Neuroanatomy: Text and Atlas*, 2nd ed. (McGraw Hill Education, New York, NY 2005).
34. Ko, H.Y., Park, J.H., Shin, Y.B. & Baek, S.Y. Gross quantitative measurements of spinal cord segments in human. *Spinal Cord* **42**, 35 (2004).
35. Brown, P.D., Davies, S.L., Speake, T. & Millar, I.D. Molecular mechanisms of cerebrospinal fluid production. *Neuroscience* **129**, 957–970 (2004).
36. Park, H.B. *et al.* Survival analysis of spinal muscular atrophy type I. *Korean J. Pediatr.* **53**, 965–970 (2010).
37. Shingleton, A. Allometry: the study of biological scaling. *Nature Educ. Knowledge.* **3**, 2 (2010).
38. Tsamandouras, N., Rostami-Hodjegan, A. & Aarons, L. Combining the “bottom up” and “top down” approaches in pharmacokinetic modelling: fitting PBPK models to observed clinical data. *Br. J. Clin. Pharmacol.* **79**, 48–55 (2015).

© 2018 The Authors *CPT: Pharmacometrics & Systems Pharmacology* published by Wiley Periodicals, Inc. on behalf of the American Society for Clinical Pharmacology and Therapeutics. This is an open access article under the terms of the Creative Commons Attribution-NonCommercial License, which permits use, distribution and reproduction in any medium, provided the original work is properly cited and is not used for commercial purposes.